Master's Thesis of Medicine

Impact of radiation dose reduction and iterative reconstruction type on musculoskeletal computed tomography: phantom study

근골격 전산화 단층촬영영상에서 iterative reconstruction 유형에 따른 방사선량 감소 효과에 대한 인체 모형 연구

February 2018

Graduate School of Medicine
Seoul National University
Radiology Major

Ji-Eun Kim

Impact of radiation dose reduction and iterative reconstruction type on musculoskeletal computed tomography: phantom study

Sung Hwan Hong

Submitting a master's thesis of Medicine

February 2018

Graduate School of Medicine
Seoul National University
Radiology Major

Ji-Eun Kim

Confirming the master's thesis written by
Ji-Eun Kim

February 2018

Chair _____(Seal)
Vice Chair _____(Seal)
Examiner _____(Seal)

Abstract

Introduction: The aim of this study was to assess the impact of radiation dose reduction and iterative reconstruction algorithms on musculoskeletal computed tomography (CT) images.

Methods: CT examinations using an anthropomorphic pelvis phantom (RS-113T, Radiology Support Devices, Long Beach, CA, USA) were performed at 80, 100, 120 kVp without dose right index (DRI) (195mAs) and with DRI (8, 14, 20) on 256-slice CT scanner (iCT256, Philips Healthcare, Cleveland, OH, USA): a total of 12 radiation dose settings. Images with bone algorithm were reconstructed with conventional filtered back projection (FBP), hybrid iterative reconstruction (iDose^4) and iterative model reconstruction (IMR). Quantitative image assessment was done with 5-times repeated measurements of signal-to-noise ratio (SNR) and contrast-to-noise ratio (CNR) in left femoral head of the phantom. Two independent blinded radiologists evaluated the images qualitatively using a 5-point scale: distinction of anatomic structures, noise, and artifact. We performed repeated-measure two-way ANOVA to evaluate the possible effect of reconstruction algorithm and radiation dose on the results of both quantitative and qualitative assessment.

Results: Although IMR was better in terms of quantitative assessments (SNR and CNR) and noise reduction, FBP and iDose^4 showed superior performance in terms of anatomical structures and artifact reduction. The images at 80 kVp showed significantly poorer quality in CNR, anatomical structures and artifact reduction. Substantial deterioration of subjective image quality was noted with lower than 50% of reference radiation dose including DRI 14 and DRI 8.

Conclusions: We recommend that the musculoskeletal CT scans

should use at least 100 kVp or DoseRightIndex (DRI) of 50% reference radiation dose as a minimum radiation dose, and iDose[4] as the reconstruction algorithm, because of their effects on reducing noise, while not significantly affecting diagnostic performance.

Keyword : computed tomography; radiation dose; dose reduction; iterative reconstruction; musculoskeletal imaging
Student Number : 2016-21952

Table of Contents

Introduction

Since the advent of multi-detector computed tomography (MDCT), the use of computed tomography (CT) has increased markedly. Although CT examination is a useful diagnostic tool in clinical practice, there are concerns about excessive radiation exposure with the increasing use of CT [1,2]. Several strategies have been suggested to reduce the radiation dose (RD) in response to these concerns [3-5]. One such strategy is the use of an iterative reconstruction (IR) technique [6-13].

Filtered back projection (FBP), a long-used 'conventional' reconstruction technique, is associated with high levels of noise and artifacts at a reduced RD [14]. Various IR techniques have been developed to overcome these limitations of FBP and to generate better images with lower noise at reduced RDs [15]. iDose^4 (Philips Healthcare, Andover, MA, USA) is a hybrid iterative reconstruction algorithm, consisting of two de noising components: an iterative maximum likelihood-type sonogram restoration, based on Poisson noise distribution, and a local structure model fitting image data that decreases the noise iteratively [7]. However, certain levels of noise and artifacts are still present. A knowledge-based IR algorithm, iterative model-based reconstruction (IMR; Philips Healthcare), is the latest-generation fully iterative IR algorithm. The IMR algorithm approaches reconstruction as an optimization process through iterative minimization of the difference between measured raw data and the estimated image via a penalty-based cost function [16]. This optimization process incorporates statistical models and system models, and it may provide further reductions in noise and artifacts [17]. Use of this novel IR technique can optimize and enhance image quality, while reducing noise [18]. Thus, it can enable a reduced RD in the CT scan without compromising image quality. According to several studies in the field of chest and abdominal CT, IMR techniques can reduce the RD by up to 80%, compared with conventional FBP [19,10]. When compared with

iDose^4, IMR also resulted in a 46-73% reduction in the RDs in CT angiography and pediatric body CT [20,11].

Despite the use of various reconstruction techniques, some worsening of the image quality is inevitable when using a lower RD. Thus, it is important to determine the degree of RD reduction without compromising diagnostic performance [21,6,22,23]. There have been concerns that low-dose CT using IR techniques may hamper diagnostic performance in studies of human abdominal CT and liver phantom CT [22,23]. However, there are also opposing views that diagnostic performance can be preserved while reducing the RD, by reducing the noise and improving edge definitions of the lesions [21,6,8]. In musculoskeletal CT imaging, there are no reported studies that evaluated the extent to which the RD can be lowered when coupled with IR techniques, compared with FBP. In addition, the characteristic watercolor-painting-like image textures of IMR are unfamiliar to some radiologists. We also concern that this IMR-specific image textures will interfere with the imaging of delicate and sharp structures in musculoskeletal imaging such as the trabecular bone and joint space. Thus, the purpose of this phantom study was to assess the impact of RD reduction and IR algorithms (iDose^4 and IMR) on musculoskeletal CT images, compared with the normal, full RD and conventional FBP reconstruction.

Materials and Methods

1. Phantom

We performed this phantom study using an anthropomorphic human pelvis phantom (RS 113T; Radiology Support Devices, Long Beach, CA, USA; Fig 1A). This pelvis phantom consisted of bone and soft tissue, but did not include visceral organs in the pelvic cavity. The phantom was 32 cm in height, measured from the superior endplate of the L1 vertebral body to the proximal diaphysis of the femur (Fig 1B). There was no pathological lesion in the phantom.

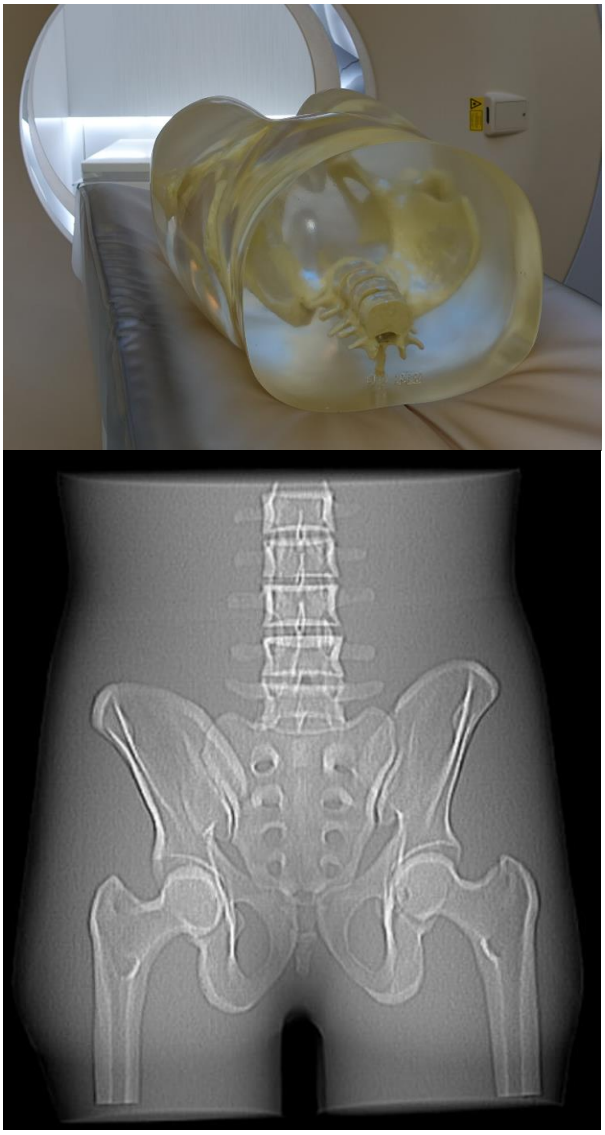

Fig 1. Appearance of the anthropomorphic human pelvis phantom.

Photograph (A). Scout image of the phantom obtained during computed tomography scan (B).

2. CT data acquisition and image reconstruction

We performed CT examinations using a 256-slice CT scanner (iCT256; Philips Healthcare, Cleveland, OH, USA). We placed the phantom at the iso-center of the scanner to avoid unnecessary noise [24]. First, the phantom was scanned at three tube voltages (80, 100, and 120 kVp) and a fixed tube current-time product (195 mAs). We subsequently repeated examinations at each tube voltage (80, 100, and 120 kVp) at three levels (12.5% , 25%, and 50% of RD) of the DoseRight Index (DRI), which provides automatic current selection, based on a reference setting of image quality [25]. Thus, 12 scan images with different RDs (three tube voltages × four tube currents) were obtained for the analysis (Table 1). The other parameters for CT examinations were kept constant as follows: detector collimation, 64 × 0.625 mm; slice thickness, 1 mm with 0.7-mm increments; gantry rotation time, 0.4 s; pitch, 0.390; scan time, 9.6 s; field of view, 400 × 400 mm; and matrix size, 512 × 512 pixels. The data acquisition started from above the superior end plate of the L2 vertebral body and proceeded down to the level of the diaphysis of the femur. The phantom was scanned once at the 12 settings, and all scan images were obtained sequentially on the same day without changing the position of the phantom.

The raw data obtained from the 12 scans were then reconstructed with three reconstruction algorithms: FBP, iDose^4 (Philips Healthcare), and IMR (Philips Healthcare). Sharp reconstruction filters were used for high-contrast regions, such as bones and joints. Thus, we obtained a total of 36 reconstruction images. For our study, iDose^4 level 2 (L2: 30%/70% blend of IR/FBP) and IMR level 1 (L1: low level of noise reduction) were chosen based on our preliminary study results; Two attending radiologists compared the overall image quality of various iteration levels of iDose^4 (from level 1 to level 7) and IMR (from level 1 to level 3) and reached consensus through combined review. Sagittal images with a 2 mm slice thickness and no increment and volume-rendering images were also reconstructed from each data set.

Table 1. Descriptive statistics for radiation dose protocols

Tube voltage (kVp)	DRI level	Tube current–time product (mAs)	CTDIvol (mGy)	DLP (mGy–cm)	Dose reduction[a] (%)
120	X	195	14.7	516.7	0
	20 (50% of RD)	113	8.4	295.3	42.8
	14 (25% of RD)	56	4.2	147.6	71.4
	8 (12.5% of RD)	29	2.2	77.3	85.0
100	X	195	8.8	309.3	40.1
	20 (50% of RD)	190	8.3	291.8	43.5
	14 (25% of RD)	95	4.2	147.6	71.4
	8 (12.5% of RD)	48	2.2	77.3	85.0
80	X	195	4.2	147.5	71.5
	20 (50% of RD)	391	8.3	291.8	43.5
	14 (25% of RD)	197	4.2	147.6	71.4
	8 (12.5% of RD)	100	2.1	73.8	85.7

DRI, DoseRight index; CTDIvol, volume CT dose index; DLP, dose–length product

[a] The degree of dose reduction of each setting was calculated compared to the images obtained at 120 kVp and 200 mAs. (B).

3. Quantitative image analysis

We calculated the signal-to-noise ratio (SNR) and the contrast-to-noise ratio (CNR) for quantitative image analysis. An attending radiologist with 3 years of clinical experience, who was blinded to RD and the reconstruction algorithm, placed circular regions of interest (ROIs) for both objects and background on axial images of the hip joint, paying attention to adjusting the area of the ROI within 150–200 mm2 (Fig 2). For the object, the medullary bone of the left femoral head was selected and, for the background, the right anterior hip soft tissue at the same level was chosen. At each ROI, the mean Hounsfield unit (HU) and standard deviation (SD) values were calculated. Thus, we obtained mean HU and SD values for both the object and background in one measurement. We repeated this measurement five times for each of the 36 reconstruction images. Using these values, we calculated SNR and CNR as follows: mean HU of the object divided by SD of the object, and mean HU of the object minus mean HU of the background divided by SD of the background, respectively. We averaged the middle three of the five values of SNR and CNR as a representative value for each image. The formulas used are as follows: $SNR = \text{Mean } HU_{Object} / SD_{Background}$, $CNR = \{(\text{Mean } HU_{Object}) - (\text{Mean } HU_{Background})\} / SD_{Background}$

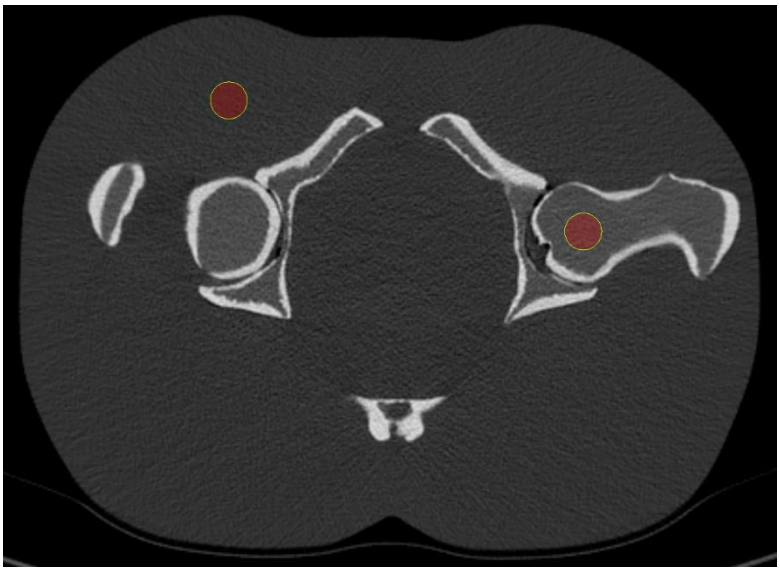

Fig 2. Quantitative image assessment.

For calculation of the signal-to-noise ratio and the contrast-to-noise ratio, circular regions of interest (ROIs) were placed at left femoral head and right anterior soft tissue of the phantom.

4. Qualitative image analysis

Two attending musculoskeletal radiologists (13 and 19 years of experience in musculoskeletal imaging, respectively) participated in the qualitative image evaluation. To improve inter-observer agreement, they were trained regarding the evaluation criteria for qualitative analysis and they practiced the grading of image quality to understand the evaluation system. We distributed the 36 reconstructed images of the phantom in random order to the two readers. They were blinded regarding the CT scan settings (tube voltage, DRI level, and reconstruction algorithm) for each image. The readers evaluated the images independently and subjectively with predefined evaluation categories, using a five-point scale.

We defined several categories to assess the quality of images comprehensively. The image evaluation categories consisted of two domains, broadly: distinction of anatomical structures, and artifacts and noise. For the distinction of anatomical structures, the readers assessed the distinction of focal cortical defects, joint space anatomy, endosteal irregularity, and thin cortical thickness, which were specifically defined in the synthetic bone of the phantom. The readers graded using a five-point scale as follows: 1 (very poor), structure not visible; 2 (suboptimal), structure only partially visible; 3 (acceptable), structure fully visible but substantial blurring of borders; 4 (good), structure fully visible but slight blurring of borders; and 5 (excellent), good depiction of structures.

For artifacts and noise, we evaluated the images in terms of beam hardening or streak artifacts on axial images, artifacts and spatial blurring on multi-planar reconstruction (MPR) images, and noise on axial and volume-rendering images. Beam hardening or streak artifacts were defined as the presence of dark streaks between two high-attenuation objects, such as bones. Dark rim artifacts on MPR images were defined as a low-attenuated rim around bones and blurring of bony edges, especially on MPR images. We also used a five-point scale to grade artifacts and noise: 1 (very poor), image very noisy and artifactual, insufficient information for a diagnosis; 2

(suboptimal), moderate noise with moderate impairment of diagnostic quality; 3 (acceptable), visible noise without impairment of diagnostic quality; 4 (good), image barely noisy or artifactual; and 5 (excellent), image neither noisy nor artifactual.

5. Statistical analyses

All statistical analyses were performed using the STATA (ver. 14; Stata Corp., College Station, TX, USA) and SPSS (ver. 22; SPSS Inc., Chicago, IL, USA) software. Agreement between the two readers regarding the qualitative image grading was determined using an intraclass correlation coefficient (ICC) analysis. First, the results of quantitative image analysis (SNR and CNR) and qualitative image analysis were compared according to the three tube voltages (80, 100, and 120 kVp) and the three reconstruction algorithms (FBP, iDose^4, and IMR), when a fixed tube current–time product of 195 mAs was used. Second, we performed comparisons again according to the four DRI levels (no DRI, 12.5%, 25% and 50% of reference RD) and the three reconstruction algorithms (FBP, iDose^4, and IMR) for each tube voltage (80, 100, and 120 kVp). We used a repeated-measures two-way analysis of variance (ANOVA), followed by a *post hoc* Bonferroni analysis. P values < 0.05 were considered to indicate statistical significance in a two-tailed test.

Results

Table 2 briefly summarizes the overall results including quantitative image analysis and qualitative image analysis.

1. Quantitative image analysis

When images were acquired without using DRI (at the fixed tube current–time product of 195 mAs), there was no significant difference in SNR or CNR, according to tube voltage, whereas there were significant differences in both, according to IR algorithm type (Table 3). They were significantly higher in images reconstructed with the IMR algorithm, versus those reconstructed with FBP (P < 0.001 for SNR and P = 0.002 for CNR) or iDose^4 (P < 0.001 for SNR and P = 0.004 for CNR) in a post hoc Bonferroni analysis. There was no significant difference between the FBP and iDose^4 algorithms in either SNR or CNR. When compared by DRI level and IR algorithm type (Table 4), SNR showed no significant difference at different DRI levels, whereas CNR did, at each tube voltage setting. SNR and CNR showed significant differences according to IR algorithm type; the IMR algorithm showed superiority versus the two other algorithms regardless of tube voltage settings (all P < 0.001). In particular, images obtained with a DRI of 12.5% RD showed significantly lower CNR than those obtained with a DRI of 50% RD (P = 0.016 for 120 and 100 kVp, and P = 0.008 for 80 kVp).

Table 2. Summary of the results

	kVp	DRI	Reconstruction algorithm
SNR and CNR	80 ≈ 100 ≈ 120	20 & 195mAs > 8 and 14	IMR > FBP and iDose
Depiction of anatomical structure	100 and 120 > 80	20 & 195mAs > 8 and 14	FBP and iDose > IMR
Artifact reduction	100 and 120 > 80	20 & 195mAs > 8 and 14	FBP and iDose > IMR
Noise reduction	100 and 120 > 80	20 & 195mAs > 8 and 14	IMR > FBP and iDose

SNR, signal to noise ratio; CNR, contrast to noise ratio; DRI, DoseRight index; FBP, Filtered back projection; IMR, Iterative model reconstruction

Table 2. Summary of the results

	kVp	DRI	Reconstruction algorithm
SNR and CNR	80 ≈ 100 ≈ 120	20 & 195mAs > 8 and 14	IMR > FBP and iDose
Depiction of anatomical structure	100 and 120 > 80	20 & 195mAs > 8 and 14	FBP and iDose > IMR
Artifact reduction	100 and 120 > 80	20 & 195mAs > 8 and 14	FBP and iDose > IMR
Noise reduction	100 and 120 > 80	20 & 195mAs > 8 and 14	IMR > FBP and iDose

SNR, signal to noise ratio; CNR, contrast to noise ratio; DRI, DoseRight index; FBP, Filtered back projection; IMR, Iterative model reconstruction

Table 3. Comparison of SNR and CNR values according to different tube voltages and different reconstruction algorithms, when DRI was not used

Tube voltage (kVp)	Signal to Noise Ratio (SNR)			Contrast to Noise Ratio (CNR)		
	FBP	iDOSE^4 L2	IMR L1	FBP	iDOSE^4 L2	IMR L1
120	3.05	4.94	13.04	3.18	4.38	11.40
100	2.03	3.49	14.66	2.68	3.97	13.48
80	1.42	2.72	12.47	2.01	3.58	15.48
P values[a]						
Tube voltage	0.188			0.847		
Reconstruction	<0.001			0.002		
	IMR vs. FBP <0.001			IMR vs. FBP 0.002		
	IMR vs. iDose <0.001			IMR vs. iDose 0.004		

SNR, signal to noise ratio; CNR, contrast to noise ratio; DRI, DoseRight index; FBP, Filtered back projection; IMR, Iterative model reconstruction; L2 level 2; L1 level 1

[a] *P* values were obtained from repeated measures two-way analysis of variance analyses. Each *P* value represents comparison by different tube voltages and comparison by different reconstruction algorithms, respectively.

Table 4. Comparison of SNR and CNR values according to different DRI levels and different reconstruction algorithms, at each tube voltage

Tube voltage (kVp)	DRI Level	Signal to Noise Ratio (SNR)			Contrast to Noise Ratio (CNR)		
		FBP	iDOSE^4 L2	IMR L1	FBP	iDOSE^4 L2	IMR L1
120	X	3.05	4.94	13.04	3.18	4.38	11.40
	20	2.35	4.19	13.44	2.72	4.05	11.17
	14	1.62	3.82	12.77	1.86	3.53	10.61
	8	0.99	3.59	14.43	1.10	3.25	10.42
P value[a]							
DRI level			0.516			0.002	
						X vs. 14 0.021	
						X vs. 8 0.004	
						20 vs. 8 0.016	
Reconstruction			<0.001			<0.001	
			IMR vs. FBP <0.001			IMR vs. FBP <0.001	
			IMR vs. iDose <0.001			IMR vs. iDose <0.001	
			iDose vs. FBP 0.023			iDose vs. FBP <0.001	
100	X	2.03	3.49	14.66	2.68	3.97	13.48
	20	1.96	3.39	14.09	3.07	4.41	13.26
	14	1.37	3.22	16.08	1.92	3.32	12.80
	8	1.05	2.78	13.85	1.21	2.95	12.84
P value[a]							
DRI level			0.303			0.008	
						X vs. 8 0.037	
						20 vs. 8 0.016	
Reconstruction			<0.001			<0.001	
			IMR vs. FBP <0.001			IMR vs. FBP <0.001	
			IMR vs. iDose <0.001			IMR vs. iDose <0.001	
			iDose vs. FBP 0.029			iDose vs. FBP 0.002	
80	X	1.42	2.72	12.47	2.01	3.58	15.48
	20	1.97	2.97	13.24	3.01	4.46	15.45
	14	1.54	2.85	13.85	1.72	3.09	15.08
	8	1.09	2.79	20.29	1.49	3.05	14.06
P value[a]							
DRI level			0.542			0.007	
						20 vs. 14 0.046	
						20 vs. 8 0.008	
Reconstruction			<0.001			<0.001	
			IMR vs. FBP <0.001			IMR vs. FBP <0.001	
			IMR vs. iDose <0.001			IMR vs. iDose <0.001	
						iDose vs. FBP 0.002	

SNR, signal to noise ratio; CNR, contrast to noise ratio; DRI, DoseRight index; FBP, Filtered back projection; IMR, Iterative model reconstruction; L2 level 2; L1 level 1; X fixed tube current of 195mAs

[a] *P* values were obtained from repeated measures two-way analysis of variance analyses. Each *P* value represents comparison by different DRI levels and comparison by different reconstruction algorithms, respectively.

2. Qualitative image analysis

For scoring in each category of subjective image evaluation, interobserver agreement was good to excellent between the two readers (ICC = 0.73-0.97; Table 5). Thus, their results were averaged for further analyses.

With the fixed 195 mAs tube current, the results comparing image quality according to tube voltage and IR algorithm are summarized in Tables 6 and 7. Distinction of the anatomical structures, except cortical thinning, artifacts on axial images, and noise showed significant differences depending on the tube voltage. Based on a post hoc Bonferroni analysis, for the distinction of focal cortical defects and joint space anatomy, images obtained with an 80 kVp tube voltage were inferior to those obtained at 100 kVp (P = 0.002 for focal cortical defects and P = 0.005 for joint space) and 120 kVp (P = 0.001 for focal cortical defect and P = 0.003 for joint space). Regarding endosteal irregularities, images at 80 kVp tube voltage were inferior to those at 120 kVp (P = 0.024) (Fig 3). Artifacts on axial images and noise on axial and volume-rendering images also increased as the tube voltage was lowered from 120 kVp to 80 kVp (P = 0.014 for beam-hardening artifacts, P = 0.016 for axial noise, and P = 0.002 for volume-rendering noise). Regarding the IR algorithm used, compared with IMR, FBP and iDose^4 showed superiority in terms of the distinction of joint space anatomy (P = 0.011 for both FBP and iDose^4) and endosteal irregularities (P = 0.024 for FBP and P = 0.016 for iDose^4) (Fig 3). Both beam-hardening artifacts and dark rim artifacts were also more effectively reduced with FBP (P = 0.040 for beam-hardening artifacts and P = 0.005 for dark rim artifacts) and iDose^4 (P = 0.040 for beam-hardening artifacts and P = 0.006 for dark rim artifact), versus IMR (Fig 4). However, IMR could effectively lower noise on both axial and volume-rendering images, compared with FBP (P = 0.003 for axial images and P = 0.002 for volume-rendering images) and iDose^4 (P = 0.008 for axial images and P = 0.006 for volume-rendering images).

Table 5. Interobserver agreement for qualitative image assessment

	ICC (95% CI)	*P* value
Focal cortical defect	0.83 (0.75–0.89)	<0.001
Joint space anatomy	0.78 (0.57–0.89)	<0.001
Endosteal irregularity	0.75 (0.52–0.87)	<0.001
Cortical thinning	0.82 (0.74–0.88)	<0.001
Beam hardening artifact	0.79 (0.58–0.89)	<0.001
Noise	0.97 (0.93–0.98)	<0.001
Spatial blurring	0.79 (0.59–0.89)	<0.001
Mach band	0.91 (0.82–0.95)	<0.001
Volume rendering noise	0.73 (0.49–0.87)	<0.001

ICC, intraclass correlation coefficient; CI, confidence interval

Table 6. Comparison of qualitative image grading regarding the distinction of the anatomical structures according to different tube voltages and different reconstruction algorithms, when DRI was not used

Tube voltage (kVp)	Focal Cortical Defect			Joint Space Anatomy			Endosteal Irregularity			Cortical Thinning		
	FBP	iDOSE^4 L2	IMR L1	FBP	iDOSE^4 L2	IMR L1	FBP	iDOSE^4 L2	IMR L1	FBP	iDOSE^4 L2	IMR L1
120	5.00	5.00	5.00	5.00	5.00	4.50	5.00	5.00	4.00	4.33	4.50	5.00
100	4.83	5.00	4.83	5.00	5.00	4.00	5.00	5.00	3.00	4.17	4.33	5.00
80	3.83	4.17	3.67	4.00	4.00	3.00	3.50	4.00	2.50	3.67	4.67	4.50
P value*												
Tube voltage		<0.001			0.002			0.018			0.393	
		120 vs. 80 0.001			120 vs. 80 0.003			120 vs. 80 0.024				
		100 vs. 80 0.002			100 vs. 80 0.005							
Reconstruction		0.210			0.006			0.010			0.058	
					FBP vs. IMR 0.011			FBP vs. IMR 0.024				
					iDose vs. IMR 0.011			iDose vs. IMR 0.016				

DRI, DoseRight index; FBP, Filtered back projection; IMR, Iterative model reconstruction; L2 level 2; L1 level 1

[a] *P* values were obtained from repeated measures two-way analysis of variance analyses. Each *P* value represents comparison by different tube voltages and comparison by different reconstruction algorithms, respectively.

Table 7. Comparison of qualitative image grading regarding the artifact and noise according to different tube voltages and different reconstruction algorithms, when DRI was not used

Tube voltage (kVp)	Artifact						Noise					
	Axial			Sagittal			Axial			Volume rendering		
	FBP	iDOSE^4 L2	IMR L1	FBP	iDOSE^4 L2	IMR L1	FBP	iDOSE^4 L2	IMR L1	FBP	iDOSE^4 L2	IMR L1
120	4.50	4.00	3.00	3.50	3.50	2.25	3.00	3.50	5.00	3.00	4.00	5.00
100	3.75	3.75	2.75	3.75	3.50	1.75	3.00	3.00	5.00	1.00	2.50	3.50
80	2.50	3.00	2.00	4.00	4.00	1.75	1.00	2.00	4.00	1.00	1.50	2.50
P value*												
Tube voltage	0.011			0.621			0.010			0.001		
	120 vs. 80 0.014						120 vs. 80 0.016			120 vs. 80 0.002		
							100 vs. 80 0.024			120 vs. 100 0.006		
Reconstruction	0.020			0.003			0.002			0.003		
	FBP vs. IMR 0.040			FBP vs. IMR 0.005			FBP vs. IMR 0.003			FBP vs. IMR 0.002		
	iDose vs. IMR 0.040			iDose vs. IMR 0.006			iDose vs. IMR 0.008			iDose vs. IMR 0.006		

DRI, DoseRight index; FBP, Filtered back projection; IMR, Iterative model reconstruction; L2 level 2; L1 level 1

[a] *P* values were obtained from repeated measures two-way analysis of variance analyses. Each *P* value represents comparison by different tube voltages and comparison by different reconstruction algorithms, respectively.

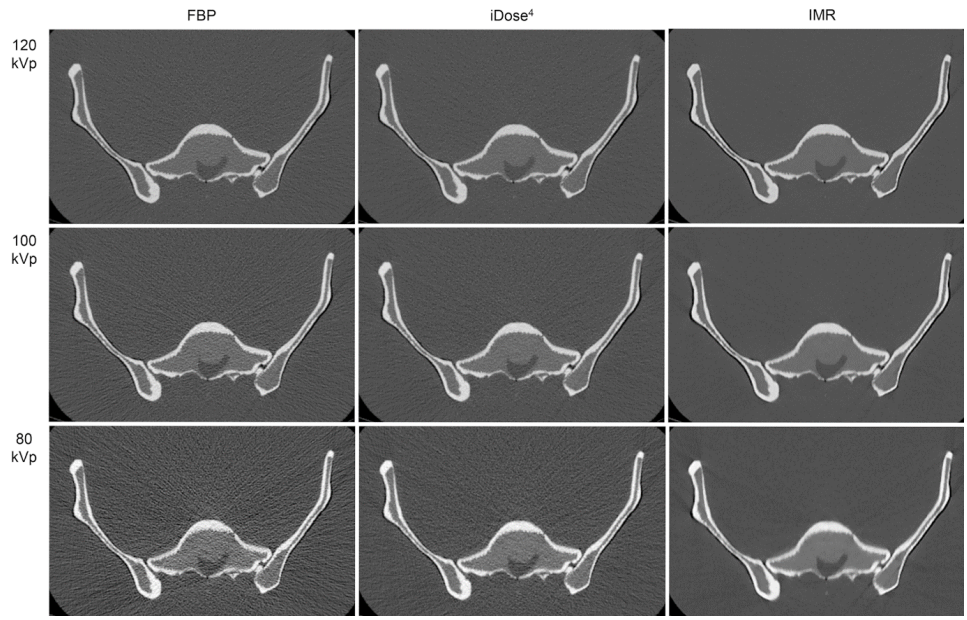

Fig 3. Qualitative image assessment of endosteal irregularity according to various levels of tube voltage at a fixed current-time product of 195 mAs.

Demonstration of fine endosteal irregularity was assessed in inner cortical plates of both iliac wings and sacrum. Each line from top to bottom corresponds to data sets related to scans acquired at 120, 100, and 80 kVp, respectively. Images are shown at an identical axial level and at the same bone window (width 2,500 HU, center 800 HU). In each line from left to right, images are reconstructed with filtered back projection (FBP), iDose^4, and iterative model reconstruction (IMR). Note that the images taken on the condition of 80 kVp (bottom row) have poor quality than those taken on the condition of 100 kVp (middle row) and 120 kVp (top row). In addition, the images of FBP or iDose^4 algorithms showed more fine demonstration of endosteal irregularity than those of IMR algorithm. calculation of the signal-to-noise ratio and the contrast-to-noise ratio, circular regions of interest (ROIs) were placed at left femoral head and right anterior soft tissue of the phantom.

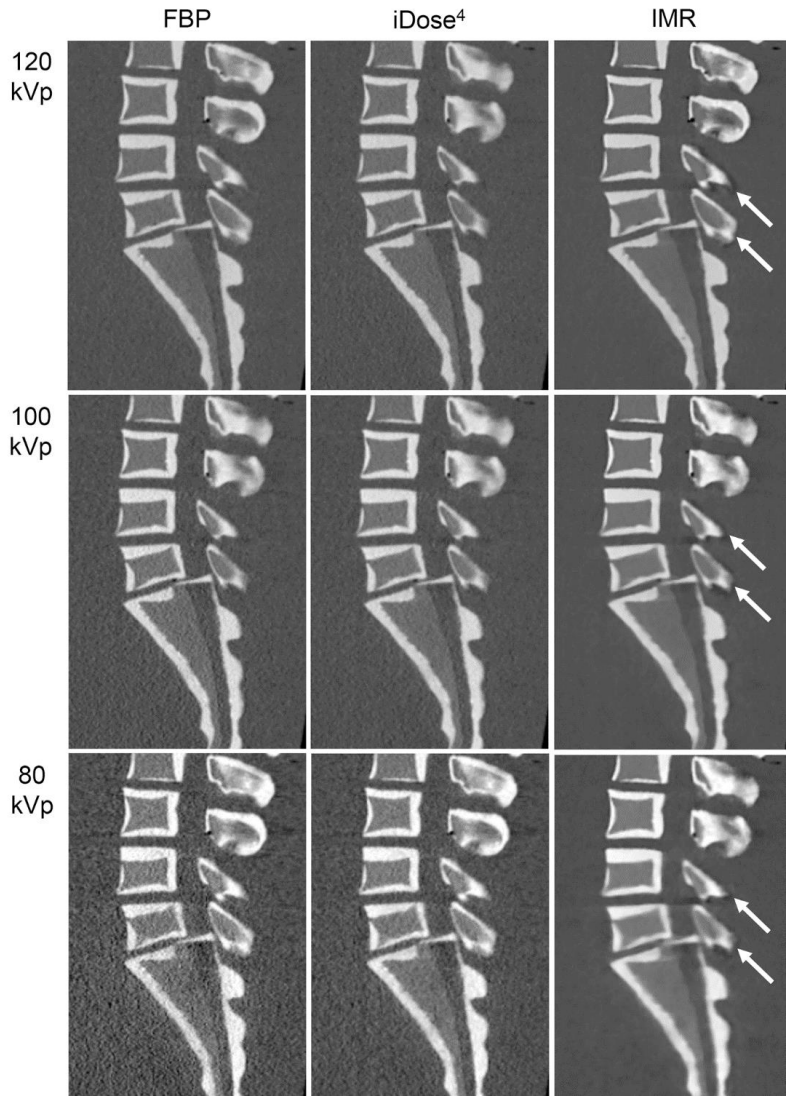

Fig 4. Qualitative image assessment of dark rim artifacts according to various levels of tube voltage.

Levels of tube voltage show no significant difference for these artifacts. Dark rim artifacts are significantly prominent with IMR (right column) than with FBP (left column) and iDose^4 (middle column). Level of tube voltage or DoseRight Index (DRI) (not shown) show no significant difference.

When the tube voltage was fixed at each of the three levels, the results comparing image quality according to DRI levels and IR algorithms are summarized in Tables 8 and 9. Distinction of anatomical structures, except focal cortical defects, differed significantly by DRI level. Regarding joint space, a DRI of 12.5% RD showed poorer performance than the others at settings of 100 and 120 kVp (P = 0.002 and 0.019, respectively), whereas DRI of 12.5% RD and 25% RD did so at a setting of 80 kVp (P = 0.009 and 0.028, respectively). Regarding endosteal irregularities, DRI of 12.5% RD and 25% RD showed inferiority to the others at each tube voltage level (P < 0.001-0.012 for 12.5% RD, and P < 0.002-0.028 for 25% RD) (Fig 5). Regarding cortical thinning, while a DRI of 12.5% RD was inferior to the others at 120 kVp, there was no significant difference at any DRI level at 80 or 100 kVp. IR algorithms showed significant differences in the distinction of anatomical structures, except focal cortical defects, regardless of the tube voltage setting. Regarding joint space and endosteal irregularities, FBP and iDose^4 showed better performance than IMR (P = 0.001-0.007 for joint space, and P = 0.002-0.016 for endosteal irregularities (Fig 5). However, IMR was superior to FBP in terms of cortical thinning (P = 0.011, 0.011, and 0.009 at 120, 100, and 80 kVp). FBP and iDose^4 showed higher performance for artifact reduction than IMR, especially for artifacts on MPR images (FBP vs. IMR; P < 0.001 for 120, 100, and 80 kVp, iDose^4 vs. IMR; P < 0.001 for 120, 80 kVp and P = 0.002 for 100 kVp). Regarding noise on axial images, IMR was superior to FBP (P = 0.003 for 120 kVp and P < 0.001 for 100, 80 kVp) and iDose^4 (P = 0.036, 0.003, and < 0.001 for 120, 100, and 80 kVp, respectively). Similarly, regarding noise on volume-rendering images, IMR showed better performance than FBP (P < 0.001 for 120, 80 kVp) or iDose^4 (P < 0.001 for 120, 80 kVp).

Table 8. Comparison of qualitative image grading regarding the artifact and noise according to different tube voltages and different reconstruction algorithms, when DRI was not used

Tube voltage (kVp)	DRI level	Focal Cortical Defect			Joint Space Anatomy			Endosteal Irregularity			Cortical Thinning		
		FBP	iDOSE^4 L2	IMR L1	FBP	iDOSE^4 L2	IMR L1	FBP	iDOSE^4 L2	IMR L1	FBP	iDOSE^4 L2	IMR L1
120	X	5.00	5.00	5.00	5.00	4.50	3.50	5.00	5.00	4.50	4.67	4.67	5.00
	20	5.00	5.00	4.83	5.00	4.50	3.50	5.00	4.50	4.00	4.50	4.67	4.83
	14	5.00	5.00	5.00	5.00	4.50	3.50	5.00	4.00	3.50	4.00	4.50	4.83
	8	4.83	4.50	3.67	4.00	4.00	2.50	4.00	3.50	3.00	3.50	4.17	4.50
P value[a]													
DRI level			0.077			<0.001			0.002			0.014	
						X vs. 8 0.002			X vs. 8 0.003			X vs. 8 0.021	
						20 vs. 8 0.002			20 vs. 8 0.012			20 vs. 8 0.046	
						14 vs. 8 0.002							
Reconstruction			0.308			<0.001			0.003			0.010	
						FBP vs. IMR <0.001			FBP vs. IMR 0.003			FBP vs. IMR 0.011	
						iDose vs. IMR <0.001							
						FBP vs. iDose 0.031							
100	X	5.00	5.00	5.00	5.00	4.50	4.00	4.50	5.00	4.00	4.67	5.00	5.00
	20	5.00	5.00	5.00	5.00	5.00	4.00	5.00	5.00	4.00	4.17	4.50	5.00
	14	5.00	5.00	4.17	5.00	4.50	3.50	4.00	4.00	3.50	3.83	4.50	5.00
	8	4.67	5.00	3.67	4.50	4.00	2.50	4.00	4.00	3.00	3.00	4.00	4.83
P value[a]													
DRI level			0.264			0.019			0.001			0.057	
						20 vs. 8 0.027			20 vs 8 0.004				
									20 vs 14 0.009				
									X vs. 8 0.009				
									X vs. 14 0.028				
Reconstruction			0.143			<0.001			0.001			0.011	

						FBP vs. IMR 0.001 iDose vs IMR 0.007			iDose vs. IMR 0.002 FBP vs. IMR 0.004			FBP vs. IMR 0.011	
80	X	4.50	4.67	4.33	5.00	4.50	3.00	4.50	5.00	4.00	3.83	4.50	4.83
	20	5.00	5.00	5.00	5.00	5.00	3.50	5.00	5.00	4.50	4.33	4.33	5.00
	14	4.67	4.83	4.50	4.50	4.00	3.00	4.00	4.00	3.50	3.83	4.50	4.83
	8	3.83	4.50	3.50	4.50	4.00	2.50	3.50	4.00	3.00	3.00	4.50	4.67
P value[a]													
DRI level			0.005			0.006			<0.001			0.351	
			20 vs. 8 0.006			20 vs. 8 0.009			20 vs. 8 <0.001				
			14 vs. 8 0.038			20 vs. 14 0.028			20 vs. 14 0.002				
									X vs.8 0.002				
									X vs. 14 0.016				
Reconstruction			0.086			<0.001			0.002			0.008	
						FBP vs. IMR <0.001			iDose vs. IMR 0.002			FBP vs. IMR 0.009	
						iDose vs. IMR <0.001			FBP vs. IMR 0.016				

DRI, DoseRight index; FBP, Filtered back projection; IMR, Iterative model reconstruction; L2 level 2; L1 level 1; X fixed tube current of 195mAs

[a] *P* values were obtained from repeated measures two-way analysis of variance analyses. Each *P* value represents comparison by different DRI levels and comparison by different reconstruction algorithms, respectively.

Table 9. Comparison of qualitative image grading regarding the artifact and noise according to different DRI levels and different reconstruction algorithms, at each tube voltage

Tube voltage (kVp)	DRI level	Artifact						Noise					
		Axial			Sagittal			Axial			Volume rendering		
		FBP	iDOSE^4 L2	IMR L1	FBP	iDOSE^4 L2	IMR L1	FBP	iDOSE^4 L2	IMR L1	FBP	iDOSE^4 L2	IMR L1
120	X	4.25	4.00	3.50	3.75	3.50	2.50	3.00	3.00	4.00	2.50	3.50	4.50
	20	4.00	4.00	2.75	3.75	3.25	2.00	2.50	3.00	4.00	2.00	3.00	4.00
	14	4.25	3.50	3.00	4.00	3.50	2.00	2.00	3.00	4.00	1.00	2.00	3.00
	8	3.50	3.50	2.50	4.00	3.75	2.00	1.00	2.50	4.00	1.00	2.00	2.50
P value*													
DRI level			0.041			0.455			0.226			0.001	
			X vs. 8 0.045									X vs. 8 <0.001	
												X vs. 14 <0.001	
												20 vs. 8 <0.001	
												20 vs. 14 0.001	
												X vs. 20 0.033	
Reconstruction			0.002			<0.001			0.003			0.001	
			FBP vs. IMR 0.002			FBP vs. IMR <0.001			FBP vs. IMR 0.003			FBP vs. IMR <0.001	
			iDose vs. IMR 0.008			iDose vs. IMR <0.001			iDose vs. IMR 0.036			iDose vs. IMR <0.001	
												iDose vs. FBP <0.001	
100	X	4.00	3.50	2.75	3.50	3.75	2.00	2.00	3.00	4.00	1.50	2.50	3.50
	20	3.75	3.50	2.50	3.75	3.00	2.00	2.00	3.00	4.00	2.00	3.50	2.50
	14	3.75	3.50	2.75	4.00	3.00	2.00	1.00	2.00	4.00	2.00	2.00	2.50
	8	2.75	3.25	3.00	3.25	3.00	1.75	1.00	2.50	4.00	1.00	2.00	2.00
P value*													
DRI level			0.572			0.390			0.094			0.195	
Reconstruction			0.041			<0.001			<0.001			0.067	
						FBP vs. IMR <0.001			FBP vs. IMR <0.001				

						iDose vs. IMR 0.002			iDose vs. IMR 0.003 FBP vs. iDose 0.008				
80	X	2.00	3.00	2.50	3.50	3.50	2.00	1.00	2.00	4.00	1.00	1.50	2.50
	20	3.50	3.50	3.00	3.75	3.25	2.25	1.50	2.50	4.00	1.50	2.50	3.50
	14	2.25	2.75	2.75	3.50	3.50	2.00	1.00	2.50	4.00	1.00	1.50	2.50
	8	3.50	3.00	2.00	3.00	3.50	1.50	1.00	2.00	4.00	1.00	1.00	2.50
P value*													
DRI level			0.268			0.240			0.189			0.005 20 vs. 8 0.009 20 vs. 14 vs. 0.021	
Reconstruction			0.422			<0.001 FBP vs. IMR <0.001 iDose vs. IMR < 0.001			0.001 FBP vs. IMR <0.001 iDose vs. IMR < 0.001 FBP vs. iDose < 0.001			<0.001 FBP vs. IMR <0.001 iDose vs. IMR <0.001	

DRI, DoseRight index; FBP, Filtered back projection; IMR, Iterative model reconstruction; L2 level 2; L1 level 1; X fixed tube current of 195mAs

[a] *P* values were obtained from repeated measures two-way analysis of variance analyses. Each *P* value represents comparison by different DRI levels and comparison by different reconstruction algorithms, respectively.

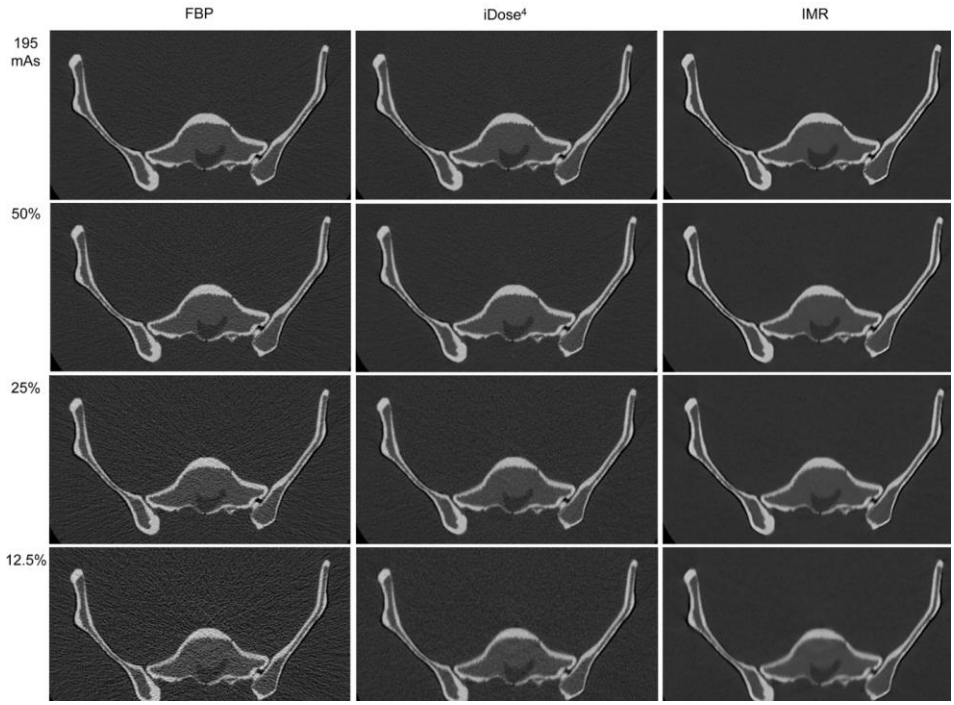

Fig 5. Qualitative image assessment of endosteal irregularity according to various levels of DoseRight Index (DRI).

Each line from top to bottom corresponds to data sets related to scans acquired at a fixed current-time product of 195 mAs, and DRI application of 50%, 25% and 12.5% of radiation dose (RD), respectively. The images of DRI 12.5% RD (bottom row) and 25% RD (second middle row) showed relatively poor demonstration of endosteal irregularity than the images of DRI of 50% RD (first middle row) and the images at 195 mAs (top row). FBP (left column) and iDose^4 (middle column) showed better performance than IMR (right column).

Discussion

We found that iDose[4] was more appropriate for reducing the RD while preserving image quality in musculoskeletal CT imaging. Images obtained with IMR were associated with poorer performance in distinguishing anatomical structures. The IMR algorithm made images with the highest SNR and CNR in our e images qualitatively, FBP and iDose[4] demonstrated finer and more precise images in terms of distinguishing anatomical structure and reducing artifacts, versus IMR. IMR had strength only in terms of noise reduction. Among the various RD settings, a tube voltage of 100 kVp (40% dose reduction versus 120 kVp) or a DRI of 50% RD (50% dose reduction versus a setting of 120 kVp and 195 mAs) showed comparable image quality, versus the ‘conventional’ settings of a tube voltage of 120 kVp and a fixed tube current−time product of 195 mAs in several of the image−evaluation categories.

Although the use of the IMR algorithm showed striking improvements in SNR, CNR, and significant noise reduction, the depiction of anatomical structures was less than ideal, especially when the RD was reduced. This finding is consistent with a previous study of low−dose abdominal CT with the IMR algorithm [26]. Thus, although reducing the RD is important, we suggest that it is also important to adjust the RD appropriately to obtain CT images of reasonable quality, so as not to reduce diagnostic performance.

Because the relationship between tube current and RD is linear, decreasing tube current by 50% will essentially decrease the RD by 50% [27]. In contrast, the relationship between tube voltage and RD is non−linear [28]. In our study, when all other parameters were held constant, and tube voltage was decreased from 120 kVp to 100 kVp (a 17% decrease), the RD decreased by ~40% for a pelvis bone phantom. Our study results suggest that RD reduction without compromising diagnostic performance is possible, with a 40% reduction in RD, at maximum, because a scan at 80 kVp (> 50%

reduction) worsened the image quality, in terms of depicting anatomical structure and artifacts. Additionally, we obtained CT images of low tube voltage in the condition of DRI application, which adjust the tube current based on the regional body anatomy for modulation of x-ray quantum noise to keep constant image noise at the lowest dose [29]. Although phantom study of various body size including large body habitus was not performed in our study, we expected that the application of automatic tube current modulation can maintain constant image quality regardless of patient's attenuation characteristics, thus allowing RD to be reduced. However, a low level of DRI of 12.5% RD or 25% RD worsened image quality significantly in terms of CNR and depicting anatomical structures. Given these results, it seems that a tube voltage of at least 100 kVp or a DRI of at least 50% RD should be used to obtain images of reasonable quality.

Interestingly, iDose^4 and IMR demonstrated superior performance in terms of the depiction of cortical thinning versus FBP in our study. When we consider that IMR was inferior in the visualization of other anatomical structures, including joint space and endosteal irregularities, compared with the other reconstruction algorithms, this result seems odd. In the IMR algorithms, an edge-preserving function is applied to maintain edges between two different attenuations. As a result, although the score for depicting a thin cortex was higher with IMR than with FBP, we suggest that IMR did not represent true cortical thickness but overestimated it.

When compared with the other IR algorithms, the unique texture of images reconstructed with the IMR algorithm may not be suitable for musculoskeletal CT images. The smooth appearance of image texture, one characteristic of IMR, can hamper the observation of delicate trabecular details. Theoretically, the outstanding capability for reducing noise with IMR may improve lesion detection and characterization with a reduced RD in CT images of other body parts [11,26,30-35]. However, in musculoskeletal CT, smooth and smudged appearances of images reconstructed with IMR can lead to a loss of perception of fine endosteal irregularities or precise joint

space anatomy. Rather, the relatively coarse texture of images reconstructed with iDose[4], due to increased image noise, may help readers to perceive anatomical details at high-contrast edges because it may reflect a more realistic osseous structure.

Our study has several limitations. First, as this study used a single anthropomorphic pelvis phantom, direct application of our study results to real humans with variable pelvic sizes is difficult. Secondly, the pelvis phantom which we used is considerably different from a human subject. It has only cortical structures without thin trabeculae within the bone. However, we think its structures are enough to evaluate cortical discontinuity such as a fracture and bone erosions. Further cadaveric or ex vivo study is warranted for a more realistic assessment. Thirdly, as we used a specific scanner with scanner-specific system optics with the IR algorithms, further studies are needed with other scanners. Finally, we did not evaluate the different model-based reconstruction methods of other vendors. Thus, a comparison among them should be performed as an independent study.

Conclusion

In conclusion, we recommend that a musculoskeletal CT should use at least 100 kVp (40% dose reduction), or a DRI of 50% dose reduction as a minimum RD, and iDose^4 as the reconstruction algorithm because of the effects in reducing noise, while not significantly affecting diagnostic performance.

References

1. Brenner DJ, Hall EJ. Computed tomography--an increasing source of radiation exposure. N Engl J Med. 2007; 357(22):2277-2284.

2. Schauer DA, Linton OW. NCRP Report No. 160, Ionizing Radiation Exposure of the Population of the United States, medical exposure--are we doing less with more, and is there a role for health physicists? Health Phys. 2009; 97(1):1-5.

3. Maher MM, Kalra MK, Toth TL, Wittram C, Saini S, Shepard J. Application of rational practice and technical advances for optimizing radiation dose for chest CT. J Thorac Imaging. 2004; 19(1):16-23.

4. Singh S, Kalra MK, Ali Khawaja RD, Padole A, Pourjabbar S, Lira D, et al. Radiation dose optimization and thoracic computed tomography. Radiol Clin North Am. 2014; 52(1):1-15.

5. Kalra MK, Maher MM, Toth TL, Hamberg LM, Blake MA, Shepard JA, et al. Strategies for CT radiation dose optimization. Radiology. 2004; 230(3):619-628.

6. Deak Z, Grimm JM, Treitl M, Geyer LL, Linsenmaier U, Korner M, et al. Filtered back projection, adaptive statistical iterative reconstruction, and a model-based iterative reconstruction in abdominal CT: an experimental clinical study. Radiology. 2013; 266(1):197-206.

7. Funama Y, Taguchi K, Utsunomiya D, Oda S, Yanaga Y, Yamashita Y, et al. Combination of a low-tube-voltage technique with hybrid iterative reconstruction (iDose) algorithm at coronary computed tomographic angiography. J Comput Assist Tomogr. 2011; 35(4):480-485.

8. Iyama Y, Nakaura T, Yokoyama K, Kidoh M, Harada K, Oda S, et al. Low-Contrast and Low-Radiation Dose Protocol in Cardiac Computed Tomography: Usefulness of Low Tube Voltage and Knowledge-Based Iterative Model Reconstruction Algorithm. J

Comput Assist Tomogr. 2016; 40(6):941-947.
9. Khawaja RD, Singh S, Gilman M, Sharma A, Do S, Pourjabbar S, et al. Computed tomography (CT) of the chest at less than 1 mSv: an ongoing prospective clinical trial of chest CT at submillisievert radiation doses with iterative model image reconstruction and iDose^4 technique. J Comput Assist Tomogr. 2014; 38(4):613-619.
10. Singh S, Kalra MK, Do S, Thibault JB, Pien H, O'Connor OJ, et al. Comparison of hybrid and pure iterative reconstruction techniques with conventional filtered back projection: dose reduction potential in the abdomen. J Comput Assist Tomogr. 2012; 36(3):347-353.
11. Smith EA, Dillman JR, Goodsitt MM, Christodoulou EG, Keshavarzi N, Strouse PJ. Model-based iterative reconstruction: effect on patient radiation dose and image quality in pediatric body CT. Radiology. 2014; 270(2):526-534.
12. Widmann G, Schullian P, Gassner EM, Hoermann R, Bale R, Puelacher W. Ultralow-dose CT of the craniofacial bone for navigated surgery using adaptive statistical iterative reconstruction and model-based iterative reconstruction: 2D and 3D image quality. AJR Am J Roentgenol. 2015; 204(3):563-569.
13. Willemink MJ, de Jong PA, Leiner T, de Heer LM, Nievelstein RA, Budde RP, et al. Iterative reconstruction techniques for computed tomography Part 1: technical principles. Eur Radiol. 2013; 23(6):1623-1631.
14. Pan X, Sidky EY, Vannier M. Why do commercial CT scanners still employ traditional, filtered back-projection for image reconstruction? Inverse Probl. 2009; 25(12):1230009.
15. Padole A, Ali Khawaja RD, Kalra MK, Singh S. CT radiation dose and iterative reconstruction techniques. AJR Am J Roentgenol. 2015; 204(4):W384-392.
16. Yuki H, Utsunomiya D, Funama Y, Tokuyasu S, Namimoto T, Hirai T, et al. Value of knowledge-based iterative model reconstruction in low-kV 256-slice coronary CT angiography. J Cardiovasc Comput Tomogr. 2014; 8(2):115-123.

17. Halpern EJ, Gingold EL, White H, Read K. Evaluation of coronary artery image quality with knowledge-based iterative model reconstruction. Acad Radiol. 2014; 21(6):805-811.
18. Volders D, Bols A, Haspeslagh M, Coenegrachts K. Model-based iterative reconstruction and adaptive statistical iterative reconstruction techniques in abdominal CT: comparison of image quality in the detection of colorectal liver metastases. Radiology. 2013; 269(2):469-474.
19. Katsura M, Matsuda I, Akahane M, Sato J, Akai H, Yasaka K, et al. Model-based iterative reconstruction technique for radiation dose reduction in chest CT: comparison with the adaptive statistical iterative reconstruction technique. Eur Radiol. 2012; 22(8):1613-1623.
20. Hansen NJ, Kaza RK, Maturen KE, Liu PS, Platt JF. Evaluation of low-dose CT angiography with model-based iterative reconstruction after endovascular aneurysm repair of a thoracic or abdominal aortic aneurysm. AJR Am J Roentgenol. 2014; 202(3):648-655.
21. Baker ME, Dong F, Primak A, Obuchowski NA, Einstein D, Gandhi N, et al. Contrast-to-noise ratio and low-contrast object resolution on full- and low-dose MDCT: SAFIRE versus filtered back projection in a low-contrast object phantom and in the liver. AJR Am J Roentgenol. 2012; 199(1):8-18.
22. Pickhardt PJ, Lubner MG, Kim DH, Tang J, Ruma JA, del Rio AM, et al. Abdominal CT with model-based iterative reconstruction (MBIR): initial results of a prospective trial comparing ultralow-dose with standard-dose imaging. AJR Am J Roentgenol. 2012; 199(6):1266-1274.
23. Schindera ST, Odedra D, Raza SA, Kim TK, Jang HJ, Szucs-Farkas Z, et al. Iterative reconstruction algorithm for CT: can radiation dose be decreased while low-contrast detectability is preserved? Radiology. 2013; 269(2):511-518.
24. McCollough CH, Bruesewitz MR, Kofler JM, Jr. CT dose reduction and dose management tools: overview of available options. Radiographics. 2006; 26(2):503-512.

25. Lee CH, Goo JM, Ye HJ, Ye SJ, Park CM, Chun EJ, et al. Radiation dose modulation techniques in the multidetector CT era: from basics to practice. Radiographics. 2008; 28(5):1451-1459.
26. Yoon JH, Lee JM, Yu MH, Baek JH, Jeon JH, Hur BY, et al. Comparison of iterative model-based reconstruction versus conventional filtered back projection and hybrid iterative reconstruction techniques: lesion conspicuity and influence of body size in anthropomorphic liver phantoms. J Comput Assist Tomogr. 2014; 38(6):859-868.
27. Frush DP, Donnelly LF, Rosen NS. Computed tomography and radiation risks: what pediatric health care providers should know. Pediatrics. 2003; 112(4):951-957.
28. McNitt-Gray MF. AAPM/RSNA Physics Tutorial for Residents: Topics in CT. Radiation dose in CT. Radiographics. 2002; 22(6):1541-1553.
29. Kalra MK, Maher MM, Toth TL, Schmidt B, Westerman BL, Morgan HT, et al. Techniques and applications of automatic tube current modulation for CT. Radiology. 2004; 233(3):649-657.
30. Eck BL, Fahmi R, Brown KM, Zabic S, Raihani N, Miao J, et al. Computational and human observer image quality evaluation of low dose, knowledge-based CT iterative reconstruction. Med Phys. 2015; 42(10):6098.
31. Gatewood MO, Grubish L, Busey JM, Shuman WP, Strote J. The use of model-based iterative reconstruction to decrease ED radiation exposure. Am J Emerg Med. 2015; 33(4):559-562.
32. Khawaja RD, Singh S, Blake M, Harisinghani M, Choy G, Karosmangulu A, et al. Ultra-low dose abdominal MDCT: using a knowledge-based Iterative Model Reconstruction technique for substantial dose reduction in a prospective clinical study. Eur J Radiol. 2015; 84(1):2-10.
33. Kim H, Park CM, Chae HD, Lee SM, Goo JM. Impact of radiation dose and iterative reconstruction on pulmonary nodule measurements at chest CT: a phantom study. Diagn Interv Radiol. 2015; 21(6):459-465.
34. Park SB, Kim YS, Lee JB, Park HJ. Knowledge-based

iterative model reconstruction (IMR) algorithm in ultralow-dose CT for evaluation of urolithiasis: evaluation of radiation dose reduction, image quality, and diagnostic performance. Abdom Imaging. 2015;
35. Ryu YJ, Choi YH, Cheon JE, Ha S, Kim WS, Kim IO. Knowledge-based iterative model reconstruction: comparative image quality and radiation dose with a pediatric computed tomography phantom. Pediatr Radiol. 2016; 46(3):303-315.

국문 초록

서론: 이 논문은 근골격계 컴퓨터단층촬영 영상에서 iterative reconstruction algorithm을 적용하였을 때 방사선량 감소에 미치는 영향을 평가하기 위한 인체유사모형 실험이다.

방법: 인체의 골반 모습을 본 딴 모형을 사용하여 세 레벨의 관전압 (80, 100, 120 kVp) 과 네 레벨의 관전류 (DoseRightIndex (DRI) 8, 14, 20, 고정관전류 195mAs) ,총 12가지의 다른 방사선 조사 조건에서 컴퓨터단층촬영 영상을 얻는다. 얻어진 영상들은 각각 filtered back projection (FBP), hybrid iterative reconstruction (iDose^4), iterative model reconstruction (IMR) 3가지의 방법으로 재구성된다. 정량적 영상 분석은 5회 반복 측정한 신호대잡음비와 대조대잡음비로 이루어진다. 정성적 영상 분석은 두 명의 영상의학과 의사가 독립적으로 참여하며, 각각 해부학적 구조물, 잡음 그리고 인공물에 대하여 5점 지표를 사용하여 분석한다. 이원반복분산분석을 이용하여 reconstruction algorithm과 방사선량이 이미지에 정량적 정성적으로 미치는 영향을 분석하였다.

결과: 세 가지의 reconstruction algorithm을 비교하였을 때 정량적 측면과 noise 감소 면에서는 IMR이 우수하였으나, 해부학적인 구조의 표현과 인공물 감소 면에서는 기존의 FBP, iDose^{4}가 더 우수하였다. 80 kVp에서 촬영된 영상은 해부학적 구조의 표현과 인공물 감소에 있어 유의하게 영상의 질이 감소하였다. 또한 기존보다 방사선량을 50% 미만으로 감소시킬 경우 정성적인 영상의 질이 상당부분 감소하는 것을 확인할 수 있었다.

결론: 이 실험 결과에 따르면 근골격계 컴퓨터단층촬영 시 적어도 100 kVp 의 관전압 혹은 DoseRightIndex (DRI) 50% 의 관전류를 최소한

의 방사선량으로 사용할 것이 추천된다. 또한 reconstruction algorithm 으로는 iDose[4]가 추천되며, 실험에 따르면 위 조건 하에서 얻은 영상은 영상의 진단적 성능을 유의하게 저하시키지 않는 범위 내에서 영상의 noise를 줄일 수 있는 것이 확인되었다.

주요어 : 컴퓨터단층촬영, 방사선량, 선량감소, iterative reconstruction, 근골격계 영상
학 번 : 2016-21952